Imaging Fluorescence of He_{2}^{*} Excimers Created by Neutron Capture in Liquid Helium II

X. Wen, S. R. Bao, L. McDonald, J. Pierce, G. L. Greene, Lowell Crow, Xin Tong, A. Mezzacappa, R. Glasby, W. Guo, and M. R. Fitzsimmons

Phys. Rev. Lett. **124**, 134502 — Published 1 April 2020

DOI: 10.1103/PhysRevLett.124.134502

Imaging Fluorescence of He_2^* Excimers Created by Neutron Capture in Liquid He II—a New Approach for Turbulent Flow Research

X. Wen,[1,2,3] S. Bao,[4,5] L. McDonald,[1,2] J. Pierce,[2] G.L. Greene,[1,2] Lowell Crow,[2] Xin (Tony) Tong,[2,6,7] A. Mezzacappa,[1,2] R. Glasby,[1] W. Guo,[4,5] and M.R. Fitzsimmons[1,2,3,*]

[1]University of Tennessee, Knoxville, TN 37996, USA.

[2]Oak Ridge National Laboratory, Oak Ridge, TN 37830, USA.

[3]Shull Wollan Center—a Joint Institute for Neutron Sciences, Oak Ridge, TN 37830.

[4]Mechanical Engineering Department, Florida State University, Tallahassee, FL 32310, USA.

[5]National High Magnetic Field Laboratory, Tallahassee, FL 32310, USA.

[6]Institute of High Energy Physics, Chinese Academy of Sciences (CAS), Beijing 100049, China.

[7]Spallation Neutron Source Science Center, Dongguan 523803, China.

*Corresponding author: M.R. Fitzsimmons mf3@ornl.gov

Abstract - We show unequivocal evidence for formation of He_2^* excimers in liquid He II created by ionizing radiation produced through neutron capture. Laser beams induced fluorescence of the excimers. The fluorescence was recorded at a rate of 55.6 Hz by a camera. The location of fluorescence was determined with an uncertainty of 5 μm. The technique provides an opportunity to record the flow of He_2^* excimers in a medium with very small viscosity and enables measurement of turbulence around macroscopic liter size objects or vortex matter in three dimensions.

A theoretical model that describes the development, intensity, and internal structure of turbulent flow remains an unsolved problem.[1] Direct numerical simulation (DNS) of individual molecules in fluid flow has produced accepted benchmarks for canonical fluid experiments (*e.g.*, flow over a smooth flat plate)[2] yet relies upon data of limited spatial and temporal resolution.[3] These limitations present a significant source of uncertainty.[4] Three dimensional (3D) velocity vector field maps are required to measure the correlation of flow around macroscopic objects in space and time under conditions of large Reynolds number (*Re*, ratio of velocity times object dimension to kinematic viscosity of the medium). These data are required to test fundamental concepts in turbulence models applied to engineering challenges[5,6,7] and to enable research in quantum turbulence related to astrophysics[8] and cosmology.[9]

The properties of liquid He II are modeled as a combination of superfluid and normal fluid components.[10,11] Their fractions can be controlled with temperature below the lambda point.[10,11,12] Yet, the viscosity of liquid He II in the range of 1 to 2 K remains roughly constant $\sim 10^{-8}\ m^2/s$,[12,13,14] which simplifies modeling flow. The small viscosity and control of the velocity of the normal component using thermal gradients, *i.e.*, thermal counter-flow,[10,11,15] or mechanical means[16] enable *Re* ~10^5 to ~10^8 to be achieved[17,18] for objects compatible with laboratory cryostats. Under steady state conditions, the mean velocity of the superfluid flow can be inferred from observation of the normal fluid flow and mass conservation.[19]

The normal flow of liquid He has been observed using μm size polymer spheres[20,21] and frozen hydrogen particles[22,23] as tracers. Particle image velocimetry (PIV)[22,24,25,26] is a technique to infer flow from motion of a high density of tracers, while particle tracking velocimetry (PTV)[22,27,28] is a technique to infer flow by individually tracking tracers usually accomplished using a low density of tracers.

Recently, electric discharge from needles[29] and lasers[15,30] have been used to ionize ^{4}He which form small "clouds" of metastable He_2^* excimers. The half-life of the excimers is 13(2) s.[31] The dimensions of the clouds formed with lasers[26] or electric discharge[15] range from 10 to 800 μm, respectively. The buoyancy and small mass of the He_2^* excimers mean that perturbations to flow caused by tracer clouds is much reduced compared to relatively massive particles. Further, excimers can be introduced into liquid He II with much less thermal

heating in comparison to introduction of massive particles. Finally, in comparison to massive particles, the binding energy of He_2^* excimers to vortex cores in superfluid He is small, so the motion and configuration of vortices in quantum matter[32] should be relatively unperturbed by the excimer tracers.[33]

To perform PIV or PTV requires production of He_2^* excimers in varying amounts, and the ability to visualize the locations of the excimer clouds to form 3D images of flow, which remain outstanding challenges. We demonstrate a new method to produce He_2^* using neutron beams and image the excimers in 2D in a manner that is readily scalable to larger length scales and 3D. The development may enable PIV and PTV analyses of measurements of flow about cm size objects, which distinguishes our approach from those that produce excimers using lasers or electric discharge. In addition, hotwire (*e.g.*, anemometry[34]) and pressure pitot tube[35] methods enable single point measurement of flow at large *Re*, while our approach is also compatible with 3D visualization of the point-to-point correlation of the velocity flow field about a macroscopic object as a function of time.

A cryostat equipped with windows transparent to 640-1100 nm light cooled a liquid ^{4}He bath to 1.7 K (Fig. 1). Laser light entered the cryostat from the left-hand side (of Fig. 1); neutrons entered from the right-hand side, and the image of the fluorescence was recorded by a camera. A glass bulb measuring $1\text{ cm} \times 1\text{ cm} \times 3.6\text{ cm}$ was inserted into the liquid He bath [Fig. 1(inset)]. The bulb was connected to a 3.5 liter reservoir with a ^{3}He:^{4}He gas ratio equal to 1:241 at a pressure of 65 kPa. When liquid ^{4}He condensed in the bath, gas from the ^{3}He:^{4}He reservoir condensed inside the bulb. This configuration enabled us to explore the dependence of the fluorescence of a liquid of constant ^{3}He:^{4}He composition.

^{3}He has a large neutron capture cross-section $\sigma = 16318 \times 10^{-24}$ cm^2 for $\lambda = 5.5$ Å wavelength neutrons.[36,37] Through the reaction $^3He + n \rightarrow {}^3H + {}^1H + 764\ keV$ a triton (191 keV) and proton (573 keV) are created. These particles ionize He which create metastable He_2^* excimers. The mean path lengths of the triton and proton in liquid He are 16 and 60 μm, respectively.[38] The energy given up by neutron capture negligibly affects the thermal energy of the liquid.[39]

Laser illumination induces fluorescence of the excimers.[30] We expect the fluorescence to be proportional to the number of excimers, thus, the fluorescence is proportional to the neutron flux and λ, because these factors determine the production rate of the ionizing radiation. A neutron beam with cross-section 1.3 cm × 1.3 cm, $\lambda = 5.5$ Å and flux $I_0 = 10^4\ ns^{-1}cm^{-2}$ illuminated the helium bath.

1 kHz pulsed light of 4 ns duration/pulse and 0.9 mJ/pulse at 905 nm from a laser was focused onto the x-z plane 1 mm wide (along y) and 10 mm tall (along z) in the center of the liquid He bath. The laser illuminated the 2 cm length of the bath (and the 1 cm length of the bulb). Owing to the transparency of liquid He to 1μm light (absorption length = $0.0135\ cm^{-1}$), the plane is uniformly illuminated (Fig. 1).

A pulse generator produced a sequence of reference pulses ["Trigger" Fig. 2(inset, left)] with frequency of 1 kHz. The first pulse triggered a light shutter to open at time t_1, then the light shutter closed after ~5 ms ["Light Shutter" Fig. 2(inset, left)]. The first, third and fifth pulses triggered the camera to take three exposures each of 10 μs duration a time t_2 after the preceding pulse ["Camera Exposure" Fig. 2(inset, left)]. A laser pulse was produced a time t_3 after every trigger pulse ["Laser Pulse" Fig. 2(inset, left)]. Light from a pair of continuous wave (CW) lasers also entered the cryostat. The purpose of the light shutter was to block the CW light from unnecessarily heating the cryostat.

Through a two-step process,[30] the 905 nm light excites He_2^* from its triplet ground state a_0 [Fig. 2(inset, right)] to an excited state d [Fig. 2(inset, right)] and decays via fluorescence of 640 nm light to state b [Fig. 2(inset, right)]. The He_2^* excimer may decay back to the triplet ground state a_0 from state b or to one of two metastable vibrational states a_1 or a_2. Excimers in metastable vibrational states cannot fluoresce until they decay into the triplet ground state—a lengthy (~2 s) process.[30] The transition time from the metastable states, a_1 or a_2, to the triplet ground state a_0 can be shortened using 1072 nm and 1097 nm CW lasers.[31]

A camera recorded the fluorescence through a band pass filter transparent to the 640 nm light but opaque to the infrared light. Images with pixel size ranging from 5.4 μm (1024×1024 pixels) to 21 μm (256×256 pixels) were taken over the camera's 5.5(1) mm by 5.5(1) mm field of view.

We quantified the influence of the laser and neutron beams and ^{3}He number density (see Supplemental Material[40]) to produce fluorescence of He_2^*. Movie 1 (see Supplemental Material[40]) shows 1000 frames collected at 55.6 Hz (Fig. 3(a)). Each frame consists of intensity measured by 256 x 256 pixels that were mapped to the camera's field of view. The intensity profiles on the lower and right sides represent the amount of charge integrated along the direction perpendicular to the side. The quasi-uniform gray color of the image is the ambient background corresponding to the gain setting of the camera and duration of the exposure. Most of the bright spots/regions correspond to fluorescence from clouds of excimers.

A background image was measured from the camera under conditions without laser light or neutrons. Fig. 2 shows the net signal (signal image – background image) integrated over the *entire* field of view as a function of time. To obtain the data in red (Fig. 2), (1) the bath was cooled to 1.7 K, (2) the neutron beam shutter was opened, and (3) after ~4 seconds, the lasers and camera were turned on. The red curve shows the variation of the net signal with time for the conditions of the lasers and neutron beams on. The decay of the net fluorescence signal, *Z*, was fitted to $Z(t) = A\, e^{-t/\tau_1} + B$ (Eq. 1), where *t* is time, τ_1 is decay time and *A* and *B* are constants. τ_1, *A* and *B* were adjusted to optimize the goodness of fit metric χ^2.[41] The solid red curve is the result for: $\tau_1 = 2.4(2)$ s, $A = 4.0(2) \times 10^{10}$ charge $\cdot$ s^{-1} $\cdot$ cm^{-2}, and $B = 2.24(4) \times 10^{10}$ charge $\cdot$ s^{-1} $\cdot$ cm^{-2} with $\chi^2 = 270$ ($\chi_\upsilon^2 = 0.3$). The net signal decays to a steady state value, *B*. For long time, there is a loss of efficiency in producing and/or detecting fluorescence. The loss may be due to some excimers being trapped in the metastable vibrational states (the a_1 and a_2 states).

The data shown in the black curve of Fig. 2 were collected starting with the lasers and camera on and the neutron beam off. At t_0 ~11 s, the neutron beam shutter was opened (the shutter opens in < 0.5 s). The increase of the net fluorescence signal, *R*, was fitted to the function that is the integral of the $e^{-t/\tau}$ portion of Eq. 1 from t_0 to t. The result is: $R(t) = \begin{cases} C, & t < t_0 \\ D\left(1 - e^{-(t-t_0)/\tau_2}\right) + C, & t \geq t_0 \end{cases}$ (Eq. 2), for: $\tau_2 = 2.8(3)\ s$, $C = 2.2(4) \times 10^9\ charge \cdot s^{-1} \cdot cm^{-2}$, and $D = 2.02(6) \times 10^{10}\ charge \cdot s^{-1} \cdot cm^{-2}$ for $\chi^2 = 188$ ($\chi_\upsilon^2 = 0.2$). C represents an underestimate of the background used in subtraction from the raw image. $B \sim C + D$, thus, the strength of the fluorescence at steady state is nearly the same for the two protocols. The variation of the black

data from zero (neutron beam off) to a non-zero value (neutron beam on) shows that neutron capture of the ^{3}He:^{4}He mixture is a necessary condition to produce fluorescence. The blue curve of Fig. 2 shows the net signal integrated over a long camera exposure time for the case of the neutron beam on and the lasers off. These data indicate the need for laser illumination to observe their fluorescence.

Focusing on the red data in Fig. 2, the decay of the signal can be understood in terms of the neutron beam first creating a large abundance of He_2^* excimers, which primarily occupy the a_0 triplet ground state, because the lasers are not yet on. The concentration of excimer clouds can be estimated to be $A_0 \sim 10^4\ clouds/cm^3$ from the beam flux, the time of a few seconds (4 s) prior to turning on the lasers, and the volume of the bulb. The excimers are confined to the liquid inside the bulb. Because the neutron absorption length of 0.4% ^{3}He in liquid ^{4}He is large $\mu = 2\ cm^{-1}$ for $\lambda = 5.5$ Å, 63% of the excimer production occurs in the region of the bulb *outside the field of view* of the camera as the neutron beam enters the bulb. 23% of the excimer production occurs inside the field of view.

Next, the lasers were turned on to produce fluorescence of the excimers. For the conditions of our experiment, we find the steady state fluorescence signal is ~33% of the maximum. The steady state value is achieved about 2.4(2) s after the lasers are turned on.

Focusing on the black data in Fig. 2, the increase of the signal can be understood in terms of the absence of excimers ($A_0 = 0\ excimers/cm^3$) before the neutron beam is turned on. Once the neutron beam is turned on, He_2^* excimers are created, and in the presence of laser light they fluoresce. With time, more excimers are created, yet because the fluorescence achieves a steady state, there must be competition between the production of excimers capable of fluorescence (those in a_0 state) and loss of these excimers. Eq. 2 represents the strength of the fluorescence at time $t > t_0$, from the superposition of excimers created from time t_0 (neutron beam on) to time t that decay with the time scale of $\tau_2 = 2.8(3)s$.

Because only the initial conditions of the two protocols (red: neutron exposure before laser illumination, black: laser illumination before neutron exposure) were changed (*i.e.*, ^{3}He concentration was constant, neutron flux constant, *etc.*), we expect the two protocols to achieve the same steady state values. Further, because the

steady state value is controlled by the rate active excimers are lost, the decay times (τ_1 and τ_2) for the two protocols should be the same. The steady state values achieved by the red and black data in Fig. 2 ($= B \sim C + D$) might be increased were the decay time longer.

From the movies (an example is Movie 1 (Ref. [40], Fig. 3(a)), we quantified the intensities, sizes and positions of the excimer clouds as a function of time. Clouds of fluorescence consist of charge recorded by the camera in a region of pixels numbering from one to several. Because the charge integrated over the field of view is dominated by background and not the occasional fluorescence, the mean of the entire measurement, ϕ, and the standard deviation above the mean, σ, were used to quantify the background. Events with peak intensity 3σ greater than ϕ were identified. For data recorded from an exposure with 1024 x 1024 pixels, approximately 2000 events per frame were identified, and about 70% of these correspond to clusters of two or more pixels. In a region of interest (ROI) that was stepped across an image, the center of mass (CM) of a single event or cluster, the standard deviation of the CM, σ_{CM}, and the net charge of the cluster (*i.e.*, charge greater than ϕ) integrated within $2\sigma_{CM}$ of the CM were computed for each event/cluster. The number of events versus net charge integrated over the duration of the exposure is shown in Fig. 4(a) (single pixel events are shown as gray). The size distribution of clusters corresponding to two or more events (numbering 90,725) in close spatial proximity (but not in the same pixel) and occurring at the same time is shown in Fig. 4(b). The average of the size distribution is 25(3) μm. This average is within the range of 10 to 60 μm expected from the mean free path of tritons and protons in liquid He and may represent a dimension characteristic of a cluster of He_2^* excimers.

The image for the *n*-th frame corresponding to fluorescence (sans background) was formed by summing events within $2\sigma_{CM}$ of the CM of each event or cluster from Movie 1 (Ref. [40]). The sequence of these images comprises Movie 2 (See Supplemental Material,[40] Fig. 3(b)). Movie 2 (Ref. [40]) represents only the fluorescence that fulfill our discrimination criterion and should reveal the velocity field through the values of the CM's corresponding to He_2^* excimers tracer clouds. These values are needed to obtain the velocity flow of the tracers with particle tracking algorithms.

In summary, we have demonstrated the ability to create numerous He_2^* excimers corresponding to the excimer cloud density of 10_4 /cm_3 in a ~ 4 cm_3 volume of liquid He. Due to the small binding energy of the excimers on quantized vortices, excimer clouds follow the motion of the viscous normal fluid in He II, thereby allowing observation of turbulence resulting from mutual friction with the superfluid component.[33] At temperatures below about 0.6 K where the excimers can bind to vortices,[32] our method may provide a non-intrusive way to introduce excimer tracers in pure superfluid for vortex imaging. The fluorescence from the excimers was recorded as images of clouds measuring ~25(3) μm in diameter and numbering ~34 per image in a 0.03 cm_3 volume defined by the camera's field of view and the 1 mm thickness of the focal plane illuminated by the lasers. This calculation suggests ~10% of the excimer production contributed towards excimer fluorescence. From Movie 2 (Ref. [40]) the sample density (of fluorescence from clouds or clusters of He_2^* excimers) in the region across the camera's field of view in the focal plane was approximately one per mm_2. The uncertainty in the extraction of the positions of centroids of the events, *i.e.*, the spatial resolution of the technique, is ~5 μm. In order to measure flow of $Re \sim 10^5$ for a cm size object in liquid He from frames separated in time by 18 ms would require tracking an excimer cloud across a separation of 2 mm—a separation too large to associate such a pair of events as being produced by the same excimer cloud.

Looking to the future we offer perspectives on how to improve the technique. From the physics perspective, the steady state rate is presently limited by the loss of excimers that are able to fluoresce. The decay time of ~3 s is much less than the 13 s half-life of the excimer; therefore, it may be possible to increase the steady state value of the fluorescence by 4×, *e.g.*, using higher power repumping lasers. Success might allow the technique to be implemented with portable neutron sources instead of a neutron facility, and the possibility to increase the sample density to one per 0.25 mm_2.

The hydrodynamics of liquid He II is controlled by phonon and roton excitations—the latter dominate at 1.7 K—and the interactions of the excitations with impurities.[42] For our experiment, the mass density of ^{3}He atoms is 0.0003 g/cm_3, while the mass density of rotons at 1.7 K is 0.033 g/cm_3.[14] Because the mass density of ^{3}He is only 0.1% of that of the rotons, we do not expect the presence of ^{3}He to affect the hydrodynamics.

From the technical perspective, the spatial and temporal resolutions are limited by the speed of the camera, and the lack of a large fast buffer to store data. With relatively straightforward improvements to the equipment, the spatial resolution can be improved from 5 to ~1μm, and the time between exposures reduced from 18 to 1 ms. Finally, with the addition of a second set of lasers and a second camera, a second plane of fluorescence can be imaged to visualize flow in 3D.

Acknowledgments

We gratefully acknowledge the experimental support of Anna Jennings and Harish Agrawal of the Neutron Scattering Division Sample Environment group, Jason Hodges of Scintillator division and Yu Zhao of the Neutron Technology Division at Oak Ridge National Laboratory (ORNL). This work was supported by the Laboratory Directed Research and Development (LDRD) Program of ORNL. ORNL is managed by UT-Battelle, LLC, for the U.S. Department of Energy under Contract No. DE-AC05-00OR22725. The research at ORNL's High Flux Isotope Reactor was sponsored by the Scientific User Facilities Division, Basic Energy Sciences, U.S. Department of Energy. X.W. acknowledges support from the Shull Wollan Center's graduate student fellowship program. S.B. and W.G. also acknowledge support from the National High Magnetic Field Laboratory, which is supported by National Science Foundation Cooperative Agreement No. DMR-1644779 and the State of Florida. W.G. acknowledges the support from the US Army Research Office under Contract No.: W911NF1910047.

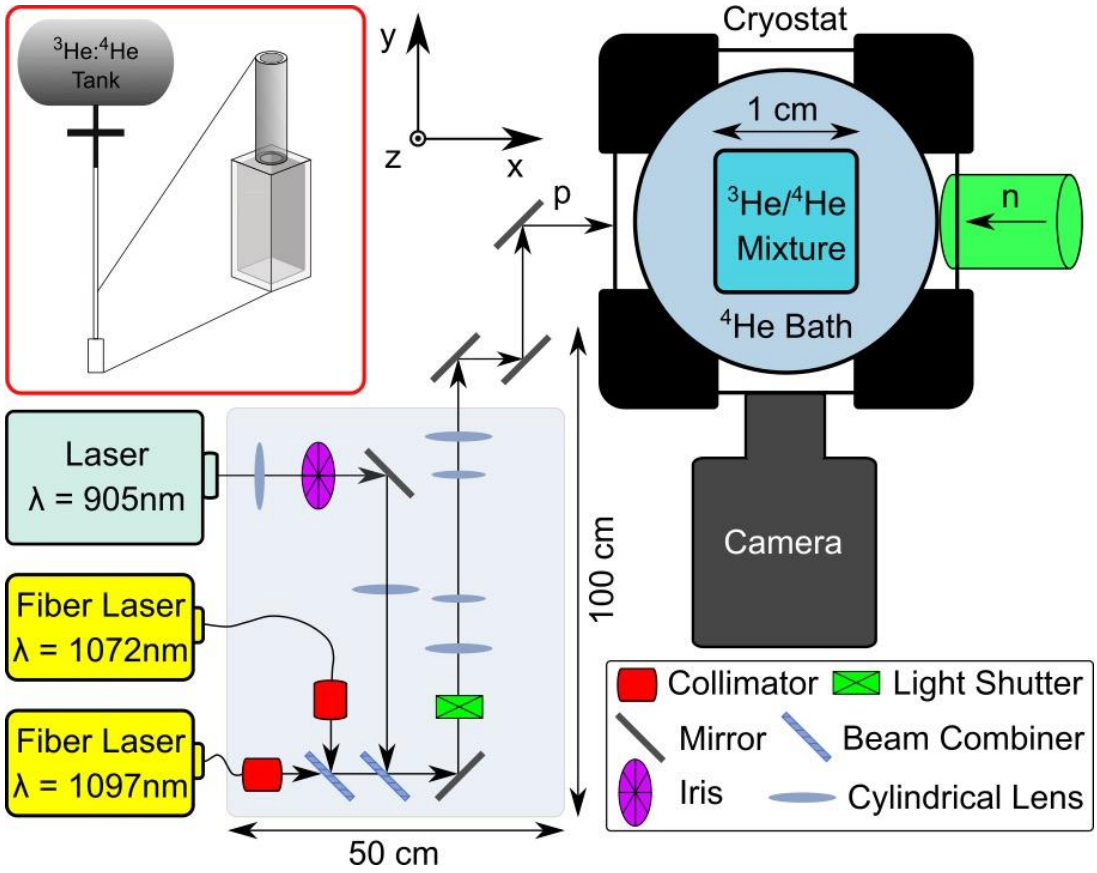

Fig. 1. Schematic of the equipment to excite fluorescence of He_2^* excimers. The position and time of the fluorescence is recorded by a camera. The figure is not shown to scale. The dimensions of the entire apparatus measures approximately 120 cm by 75 cm by 30 cm. The camera's lateral field of view is 5 mm by 5 mm. (inset) Schematic of the ^{3}He:^{4}He reservoir and bulb.

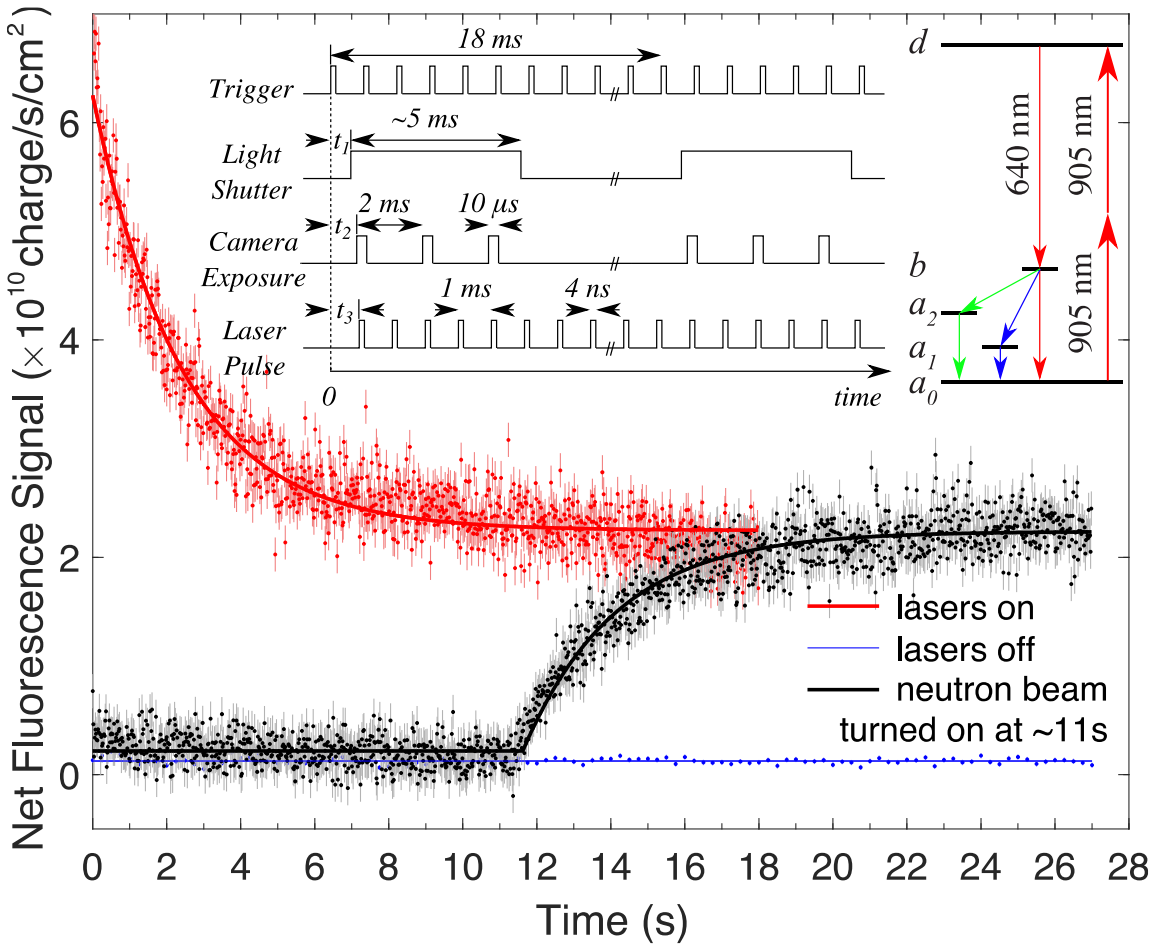

Fig. 2. (red) Neutron beam on prior to lasers being turned on at time = 0. (blue) For neutron beam on and lasers off. (black) Lasers on, neutron beam off, then turned on at time ~11s. The bars represent 3σ errors. The solid curves are fits to functions discussed in the text. (inset, left) Timing diagram of the experiment. (inset, right) Excimer transition scheme adapted from Ref. [29].

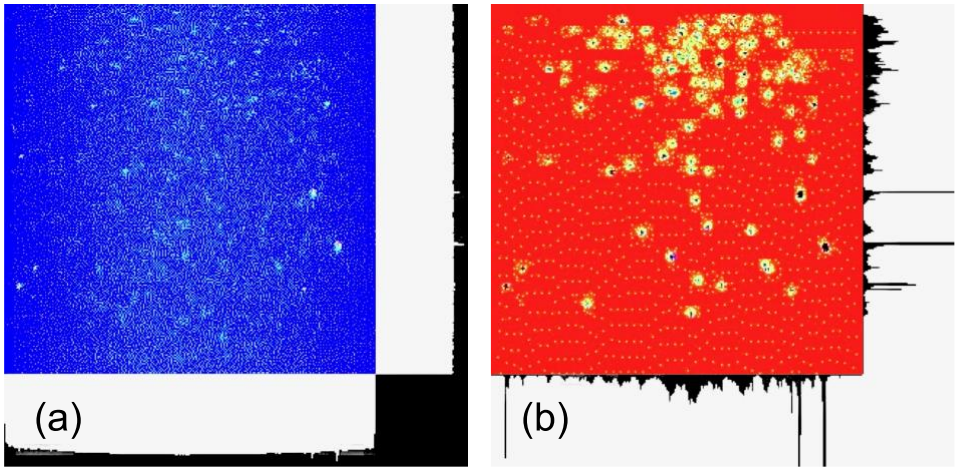

Fig. 3. Screenshots of the first image of (a) Movie 1 (raw movie) and (b) Movie 2 (synthesized from the peak finding algorithm). See Supplemental Material (Ref. [40]).

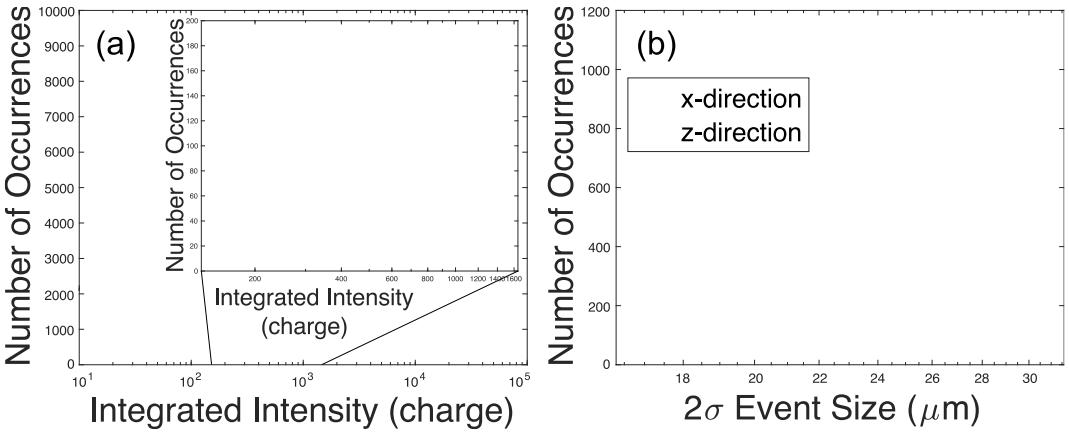

Fig. 4. Distributions of (a) integrated intensity and (b) size of events. Data are recorded in a field of view mapped to 1024 x 1024 pixels in 50 exposures of 10 μs each.

References

[1] I. Eames and J.B. Flor, *New developments in understanding interfacial processes in turbulent flows*. Phil. Trans. R. Soc. A, **369** 702-705 (2011).

[2] P. Lammers, K. N. Beronov, R.Volkert, G.Brenner and F. Durst, *Lattice BGK direct numerical simulation of fully developed turbulence in incompressible plane channel flow*. Computers & Fluids, **35**, 1137-1153 (2006).

[3] P. K. Yeung, K. R. Sreenivasan, and S. B. Pope, *Effects of finite spatial and temporal resolution in direct numerical simulations of incompressible isotropic turbulence*. Phys. Rev. Fluids, **3** 064603 (2018).

[4] T. A. Oliver, N. Malaya, R. Ulerich, and R. D. Moser, *Estimating uncertainties in statistics computed from direct numerical simulation*. Physics of Fluids, **26** 035101 (2014).

[5] F.G. Schmitt, *About Boussinesq's turbulent viscosity hypothesis: historical remarks and a direct evaluation of its validity*. Comples Rendus Mécanique, **335** 617-627 (2007).

[6] L. Prandtl, *Bericht uber Untersuchungen zur ausgebildeten Turbulenz.* Z Angew. Math Mech, **5** 136-139 (1925).

[7] J. Smagorinsky, *General circulation experiments with the primitive equations*. Monthly Weather Review, **91** 99-164 (1963).

[8] D. Page, M. Prakash, J. M. Lattimer, and A. W. Steiner, *Rapid Cooling of the Neutron Star in Cassiopeia A Triggered by Neutron Superfluidity in Dense Matter*. Phys. Rev. Lett., **106** 081101 (2011).

[9] C. Bäuerle, Yu. M. Bunkov, S. N. Fisher, H. Godfrin and G. R. Pickett, *Laboratory simulation of cosmic string formation in the early Universe using superfluid ^{3}He.* Nature, **382** 332-334 (1996).

[10] W.F. Vinen, *The physics of superfluid helium*, in CAS - CERN Accelerator School on Superconductivity and Cryogenics for Accelerators and Detectors, Erice, Italy, 8 - 17 May 2002, pp.363-373 (CERN-2004-008).

[11] W.F. Vinen, *An Introduction to Quantum Turbulence*. J. Low Temp. Phys., **145** 7-24 (2006).

[12] J.G. Dash and R.D. Taylor, *Hydrodynamics of Oscillating Disks in Viscous Fluids: Density and Viscosity of Normal Fluid in Pure He^4 from 1.2°K to the Lambda Point.* Phys. Rev., **105** 7 (1955).

[13] J.T. Tough, W.D. McCormick and J.G. Dash, *Viscosity of Liquid He II.* Phys. Rev., **132** 2373 (1963).

[14] R.J. Donnelly and C.F. Barenghi, *The Observed Properties of Liquid Helium at the Saturated Vapor Pressure.* J. Phys. Chem. Ref. Data, **27** 1217 (1998)

[15] W. Guo, S. B. Cahn, J. A. Nikkel, W. F. Vinen, and D. N. McKinsey, *Visualization Study of Counterflow in Superfluid ^{4}He using Metastable Helium Molecules*. Phys. Rev. Lett., **105** 045301 (2010).

[16] P.M. McConnell, *Liquid Helium Pumps*. National Bureau of Standards Interim Report NBSIR pp. 73-316 (1973).

[17] R.J. Donnelly and K.R. Sreenivasan, *Flow at Ultra-High Reynolds and Rayleigh Numbers: A Status Report* (Springer-Verlag, New York 1998).

[18] R.J. Donnelly, *High Reynolds Number Flows Using Liquid and Gaseous Helium* (Springer-Verlag, New York 1991).

[19] M. E. Hayden, G. Archibald, P. D. Barnes, W. T. Buttler, D. J. Clark, M. D. Cooper, M. Espy, R. Golub, G. L. Greene, S. K. Lamoreaux, C. Lei, L. J. Marek, J.-C. Peng, and S. I. Penttila, *Neutron-Detected Tomography of Impurity-Seeded Superfluid Helium.* Phys. Rev. Lett., **93** 105302 (2004)

[20] T. Zhang and S.W. Van Sciver, *Large-scale turbulent flow around a cylinder in counterflow superfluid ^{4}He (He (II)).* Nature Physics, **1** 36-38 (2005).

[21] T.Zhang, D. Celik and S.W. Van Sciver, *Tracer Particles for Application to PIV Studies of Liquid Helium*. Journal of Low Temperature Physics, **134** 985-1000 (2004)

[22] J. Xu, K.M. Smith, D. Celik, M.Y. Hussaini and S.W. Van Sciver, *Hydrogen particles in liquid helium*, Cryogenics, **44** 507-514 (2004).
[23] G.P. Bewley, K.R. Sreenivasan and D.P. Lathrop, *Particles for tracing turbulent liquid helium.* Experiments in Fluids, **44** 887-896 (2008).
[24] M. Raffel, C.E. Willert, F. Scarano, C.J. Kähler and S.T. Wereley, *Particle Image Velocimetry—A Practical Guide* (Springer, Berlin, 2007).
[25] R. J. Donnelly, A.N. Karpetis, J.J. Niemela, K.R. Sreenivasan, W.F. Vinen, and C.M. White, *The Use of Particle Image Velocimetry in the Study of Turbulence in Liquid Helium*. J. Low Temp. Phys., **126** 327-332 (2002).
[26] W. Guo, M. La Mantia, D. P. Lathrop, and S. W. Van Sciver, *Visualization of two-fluid flows of superfluid helium-4.* PNAS, **111** 4653-4658 (2014).
[27] T. Dracos, Particle Tracking Velocimetry (PTV) in *Three-Dimensional Velocity and Vorticity Measuring and Image Analysis Techniques* ERCOFTAC Series 4, T. Dracos editor, (Springer, Dordrecht, 1996) pp. 155-160.
[28] B. Sokoray-Varga and J. Józsa, *Particle tracking velocimetry (PTV) and its application to analyse free surface flows in laboratory scale models*. Periodica Polytechnica Civil Engineering, **52** 63-71 (2008).
[29] W. Guo, J. D. Wright, S. B. Cahn, J. A. Nikkel, and D. N. McKinsey, *Metastable Helium Molecules as Tracers in Superfluid ^{4}He.* Phys. Rev. Lett., **102** 235301 (2009).
[30] A. Marakov, J. Gao, W. Guo, S. W. Van Sciver, G. G. Ihas, D. N. McKinsey, and W. F. Vinen, *Visualization of the normal-fluid turbulence in counterflowing superfluid ^{4}He*. Phys. Rev. B, **91** 094503 (2015).
[31] W. G. Rellergert, S. B. Cahn, A. Garvan, J. C. Hanson, W. H. Lippincott, J. A. Nikkel, and D. N. McKinsey, *Detection and Imaging of He_2 Molecules in Superfluid Helium.* Phys. Rev. Lett., **100** 025301 (2008).
[32] D. E. Zmeev, F. Pakpour, P. M. Walmsley, A. I. Golov, W. Guo, D. N. McKinsey, G. G. Ihas, P. V. E. McClintock, S. N. Fisher, and W. F. Vinen, *Excimers He^*_2 as Tracers of Quantum Turbulence in ^{4}He in the T = 0 Limit.* Phys. Rev. Lett., **110** 175303 (2013).
[33] W. Guo, *Molecular Tagging Velocimetry in Superfluid Helium-4: Progress, Issues, and Future Development.* J. of Low Temp. Phys., **196** 60-72 (2019).
[34] M. Hultmark, M. Vallikivi, S. C. C. Bailey, and A. J. Smits, *Turbulent Pipe Flow at Extreme Reynolds Numbers.* Phys. Rev. Lett., **108** 094501 (2012).
[35] S. C. C. Bailey, M. Hultmark, J. P. Monty, P. H. Alfredsson, M. S. Chong, R. D. Duncan, J. H. M. Fransson, N. Hutchins, I. Marusic, B. J. McKeon, H. M. Nagib, R. Örlü, A. Segalini, A. J. Smits and R. Vinuesa, *Obtaining accurate mean velocity measurements in high Reynolds number turbulent boundary layers using Pitot tubes.* J. Fluid Mech., **715** 642-670 (2013).
[36] S. Falahat, A. Best, M. Couder, J. Görres, K. Kratz, U. Ott, Ed Stech, M. Wiescher, *A ^{3}He neutron detector for the measurement of (α,n) Reactions.* Nucl. Instr. and Methods in Phys. Res. A, **700** 53-58 (2013).
[37] A. Rauch and W. Waschkowski, Neutron Properties in *Neutron Data Booklet*, eds. Albert-Jose Dianoux and Gerry Lander (Institut Laue-Langevin, Grenoble 2002) pp. 1.1-4.
[38] C.F. Williamson, J.P. Boujot, J. Picard, *Tables of range and stopping power of chemical elements for charged particles of energy 0.05 to 500 MeV.* Rapport Centre D'Etudes Nucleaires de Saclay, CEA-R3042 pp. 3-151 (1966).
[39] M.J. Buckingham and W.M. Fairbank, *Chapter III The Nature of the λ-Transition in Liquid Helium.* Progress in Low Temperature Physics, **3** 80-112 (1961).
[40] See Supplemental Material at *"LINK"* for further details on experimental methods, movies, the influence of neutron flux and quantity of ^{3}He on the net fluorescence signal.
[41] W.H. Press *et al., Numerical Recipes, The Art of Scientific Computing* (Cambridge University Press, London (1986)), p. 470.

[42] T.M. Sanders Jr, *Semiclassical mechanics of rotons*. Contemporary Physics, **42** 151-157 (2001).